JOURNAL OF SPACECRAFT AND ROCKETS
Vol. 43, No. 1, January–February 2006

Simulation of Missiles with Grid Fins Using an Actuator Disk

P. Reynier* and J. M. Longo*
DLR, German Aerospace Center, 38108 Braunschweig, Germany
and
E. Schülein†
DLR, German Aerospace Center, 37073 Göttingen, Germany

An actuator disk for grid fin simulations has been integrated in the DLR, German Aerospace Center's TAU unstructured code. With this method, the physical grid fins are replaced by artificial boundary conditions in the flow for the numerical simulations. The objective in using an actuator disk is to reduce the computational effort during the design loops of vehicles equipped with grid fins. The forces produced by the grid fins are computed using a procedure based on the semiempirical theory for lattice wings and coupled with the code. The final tool is applied to the predictions of force and moment coefficients around a missile with grid fins. The numerical predictions are compared with the experimental data obtained at DLR for a Mach number range from 1.8 to 4 and different angles of attack. In addition, computations for a body alone have been performed to be used as a reference to assess the code capabilities in recovering the experimental differences of force and moment coefficients between the complete missile and the body alone. The results for several Mach numbers show the capability of the method to predict the differences found experimentally between the drag of the vehicle and the body. The numerical simulations with angle of attack show good agreement with the experiments for force coefficients and pitching moment. The capabilities of the tool at different Mach numbers and angles of attack and its usefulness for the design of vehicles equipped with grid fins are shown.

Nomenclature

b	=	grid fin span
C_d	=	drag coefficient
C_m	=	pitching moment
C_x	=	axial force coefficient
C_z	=	normal force coefficient
c	=	plane thickness of grid fin
c_f	=	skin-friction coefficient
c_x	=	axial force coefficient
c_{x_f}	=	axial friction coefficient
c_{x_i}	=	axial lift coefficient
c_{x_p}	=	integrated surface pressure force coefficient
c_{x_w}	=	axial wave drag coefficient
h	=	grid fin height
M	=	Mach number
M_{cr1}	=	first critical Mach number
M_{cr2}	=	second critical Mach number
M_{cr3}	=	third critical Mach number
n	=	number of cells in grid fin
S_x	=	surface area of grid fin perpendicular to x direction
S_y	=	surface area of grid fin perpendicular to y direction
S_z	=	surface area of grid fin perpendicular to z direction
s	=	thickness of grid fin internal frame
t	=	thickness of grid fin external frame
t_y	=	horizontal size of lattice wing cell
t_{yz}	=	size of square lattice wing cell
t_z	=	vertical size of lattice wing cell
x, y, z	=	Cartesian coordinates
y^+	=	dimensionless value of y

Received 29 January 2004; revision received 2 February 2005; accepted for publication 3 February 2005.

*Research Engineer, Institut für Aerodynamik und Strömungstechnik, Lilienthalplatz 7.

†Research Engineer, Institut für Aerodynamik und Strömungstechnik, Bunsenstrasse 10.

Introduction

SINCE the mid-1980s, lattice wings, also called grid fins or lattice controls, have been the object of a strong interest in the scientific community working on missile technology. In 1998, several papers presented at the Applied Vehicle Technology Panel Symposium held in Sorrento, Italy, were focused on this topic.[1–4] Other studies on lattice wings have been carried out in Canada, Russia, Taiwan, and the United States. Some were dedicated to experimental investigations,[5–7] others to theoretical analysis[8,9] or to numerical computations of missiles with lattice wings.[10–12] Some investigations were dedicated on the experimental investigation of an isolated lattice wing[13] and the numerical simulation of the flow inside a grid fin cell.[14]

The aerodynamic qualities of grid fins have been known for a long time and have already been listed.[4] They are very effective control devices and sometimes have advantages over planar fins.[4] Their performance in the supersonic regime and their relatively small size make them very attractive for missile applications. They present two main disadvantages: They suffer a loss of stability in the transonic regime and have relatively high drag levels. The first disadvantage[3] occurs because the grid fin cells choke in the transonic regime. The high drag levels of grid fins has been the main concern that has for many years restricted the use of this technique. However, recently, some experimental studies[15] have shown that grid fin drag levels can be considerably reduced by altering the frame cross-section shape and the web thickness with only a minimal impact on lift and other aerodynamic properties.

Several numerical studies[10–12] have been dedicated to flow simulation of vehicles equipped with grid fins. Generally, the results show that Navier–Stokes computations of missiles with grid fins compare well with experimental data. The same investigations have highlighted that the predictions obtained with an Euler approach were not appropriate for these flows. However, the Navier–Stokes simulations are expensive due to the complexity of the geometry, which requires 80% of the mesh to be located in the grid fin region.[10]

Since the 1990s, different research activities on grid fins have been conducted in Germany. This topic has focused the interest of DLR, German Aerospace Center,[16] but also of industry[17] for high-supersonic missiles. In the past years, several test campaigns have been led[18] to investigate different geometries of lattice wings and missiles with grid fins to create a large experimental database

devoted to these controls. In parallel to these experiments, numerical investigations have been undertaken. To save some computational effort, a methodology based on the actuator disk technique has been developed[19,20] to simulate flows around a vehicle with lattice wings. In this approach, the lattice wings are replaced by an actuator disk and, therefore, by artificial boundary conditions inside the flow, where the forces produced by the grid fins are taken into account in the balance equations. Initially, this method[19,20] was coupled to an experimental database providing the force coefficients at the lattice wing locations. Several simulations have been performed for an isolated grid fin[19] and a complete vehicle[20] experimentally investigated by Esch.[18] The comparisons with the experimental data[20] have demonstrated the capabilities of the method, but also the strong dependence of the numerical result reliability on the database range of validity.

The actuator disk for lattice wings is now integrated in the TAU[21] unstructured solver developed by DLR. This allows some new savings of mesh generation effort. In the current study, the actuator disk has not been coupled with an experimental database but with a numerical procedure based on the semiempirical theory for lattice wings.[8] In this procedure, the forces at the lattice wing location are computed as functions of geometrical parameters and flow conditions using semiempirical formulas. The numerical tool has already been successfully applied to the prediction of the force coefficients of an isolated grid fin.[22] In the current effort, the code is applied to the prediction of the aerodynamic performance, in terms of force and moment coefficients, of a complete vehicle. This will assess the capacity of the tool to be used for the design of high-supersonic vehicles equipped with grid fins.

Numerical Aspects

Flow Solver

The code TAU,[21] developed by DLR, has been used for the numerical simulations. It solves the three-dimensional Navier–Stokes equations, written in a conservative form, using a finite volume approach, and can handle structured, unstructured, and hybrid meshes built with prisms, pyramids, tetrahedra, and hexaedra. Different numerical schemes are available for the flux discretization using upwind (AUSM, Roe, Van Leer) or central discretization (scalar or matrix dissipation). Dissipation terms are also added to damp high-frequency oscillations. For the current study, the AUSM-DV scheme has been retained. The final scheme is accurate to the second order in space. The integration in time is carried out through an explicit Runge–Kuttta scheme. For accelerating the convergence, techniques like local time stepping, residual smoothing, and multigrid are available. They have been used for the current computations. Transition modeling, as well as different turbulence models, are incorporated in the code; among others, the Baldwin–Lomax, Spalart–Allmaras, and k–w model can be cited. Unsteady flows can also been handled by the code, and special features such as grid deformation and large eddy simulation can be used. Additional numerical techniques like chimera and low Mach number preconditioning are also incorporated in the code. A module for grid adaptation is also available and has been used to check the grid dependence of the results. This tool is vectorized and parallelized.

Actuator Disk

An actuator disk is an artificial discontinuity inside a flow. This theory has been extensively described by Horlock.[23] According to Horlock, this concept dates back to the Rankine–Froude theory of the flow through a ship propeller. Since then, the actuator disk concept has been used to model a wide range of engineering problems such as helicopter rotors, windmills, or multistage turbomachines. Here, this technique is applied to model lattice wing effects for predicting the flow around a missile with grid fins. To reduce the computational cost of the simulations around this geometry, an actuator disk has been initially developed.[19,24] The geometrical details of the missile and the grid fins are represented in Figs. 1 and 2. By the use of an actuator disk, each lattice wing is replaced by a set of artificial boundary conditions inside the flow.[19,20]

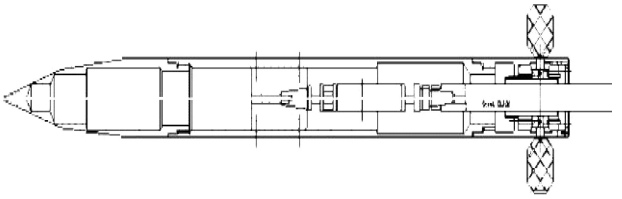

Fig. 1 Missile with lattice wings experimentally investigated by Esch,[18] wings parallel to body for visualization purposes.

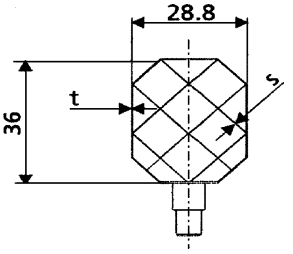

Fig. 2 Grid fin with its support, experimentally investigated by Esch and studied numerically here: $s = 0.50$ mm, $t = 0.50$ mm, $s_Z = 877$ mm^2, $s_Y = 939$ mm^2, and $s_X = 159$ mm^2.

The actuator disk theory is based on the application of the conservation laws for mass, momentum, and energy. With this technique, the grid fin is replaced by two sets of boundary conditions. At the upstream side of the actuator disk, the characteristic theory is applied. Therefore, all of the variables are extrapolated for a supersonic flow, whereas one has to be imposed for a subsonic flow. Here, for a subsonic flow, the density and velocity components are extrapolated from inside the domain, and the mass flux is chosen as the variable to be prescribed. Its value at the downstream boundary of the actuator disk is imposed, whereas pressure and energy are calculated supposing that the total enthalpy remains constant.

The characteristic theory is also used at the downstream side of the actuator disk. As a consequence, four flow properties have to be imposed if the flow is subsonic, whereas the fifth is extrapolated from inside the flowfield. The velocity has been chosen as the variable to be extrapolated. For a supersonic flow, all of the variables have to be imposed. In this case, all of the flow variables at the downstream boundary are calculated from their respective values at the upstream boundary of the actuator disk. The local aerodynamic forces produced by the presence of the grid fin are accounted for in the flux balance at the downstream side of the actuator disk. These forces are computed with a semiempirical module, described hereafter, as functions of the local flow conditions and geometrical parameters.

These boundary conditions, developed for laminar flows, have been extended to turbulent flows using Neumann boundary conditions for the turbulent quantities at the actuator disk. Of course, this is a very rough approximation that does not account for the impact of the lattice wing on the turbulence. The clarification of this point, which would be an important target for a future study, has not been examined here.

Semi-Empirical Module

Downstream of the actuator disk, the flow characteristics are changed due to the impact of the lattice wing. With dependence on grid fin geometry and local flow conditions in terms of Mach number and pitch and yaw angles, this impact has to be determined. For the previous studies[19,20] carried out with the actuator disk for lattice wings, the force coefficients were interpolated from a database. This allowed an estimate of the resulting forces and moments induced by the lattice wing. The database was obtained from wind-tunnel experiments[18] obtained for the isolated grid fin of Fig. 2, which is identical to those used for the complete missile of Fig. 1. This database covered a supersonic range of Mach numbers from 1.8 to 4.

The results reported in Fig. 3 show that, even with a database valid for the current grid fin, the approach was not capable of recovering more than 75% of the drag for the total vehicle for all computed Mach numbers. This was due to slight velocity deviations around

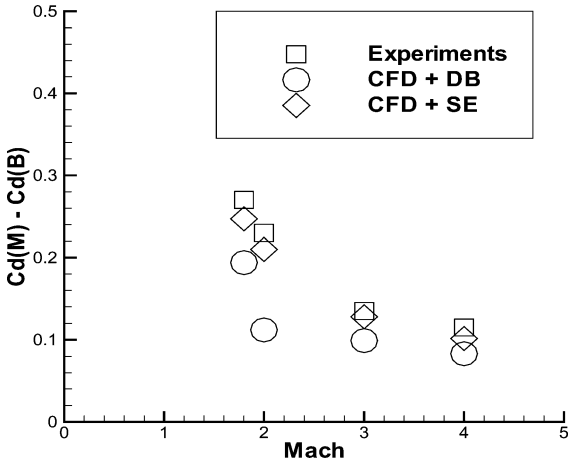

Fig. 3 Differences between drags of complete missile and body obtained experimentally (Experiments), numerically with database (CFD + DB),[19] and with semiempirical module (CFD + SE) in current work.

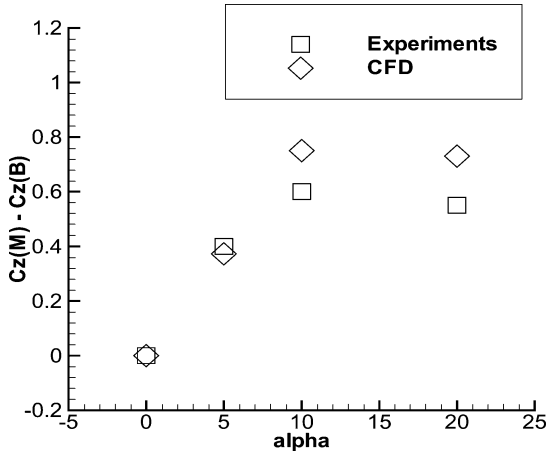

Fig. 4 Differences between normal forces of complete vehicle and body alone at Mach 1.8, in experiments[18] and in numerical simulations.[24]

the grid fin induced by the presence of the body. The grid fin/body interactions create local conditions in terms of Mach number, angle of attack, and yaw angle. As a consequence, the local interpolated force coefficients of the fin were not perfectly suited for the computed cases.

This situation was, of course, much worse in presence of an angle of attack, particularly in the range of Mach numbers where nonlinear effects are strong. The numerical predictions for a complete missile in presence of high angle of attack[19,20] showed some strong discrepancies with the experiments.[18] These discrepancies can be observed in Fig. 4, where the differences between the normal forces of the complete vehicle and the body alone are plotted for the numerical simulations and the experiments. The discrepancies were strong for angles of attack higher than 10 deg. These differences were induced by the presence of a vortical flow developing along the missile and impacting on one lattice wing. This is highlighted in Fig. 5, which shows the vortical flow along the missile at a 10-deg angle of attack. This points out the source of the discrepancies: The database used was not valid in the presence of vortical flow because the resulting local flow conditions were transonic, whereas the database was only covering a Mach number range from 1.8 to 4. The previous investigation demonstrated the strong dependence of the reliability of the numerical results on the database.

Here, to extend the applicability of the method, the actuator disk is coupled with a numerical module,[25] mainly based on a semiempirical theory for lattice wings. In this theory,[8] which is the result of extensive experimental and numerical investigations, the

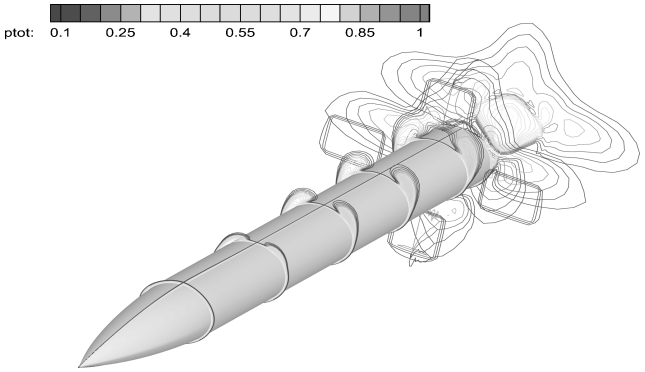

Fig. 5 Total pressure distribution around complete vehicle (turbulent flow, Mach 1.8, 10-deg angle of attack) simulated by Reynier et al.[24] with several planes in transversal direction.

force coefficients of the grid fins are computed using semiempirical relations. The experimental results obtained at DLR[16,18] for basic lattice wing configurations and a wide range of Mach numbers and angles of attack have been used to complete and modify this theory, which can be briefly described as follows. With regard to the current effort, the semiempirical method allows the development of a predictive capability for high-supersonic flight, which could not be addressed using the existing experimental database.

The calculation of the grid fin performance takes advantage of the fact that, at all Mach numbers, the critical angle of attack corresponding to the maximum lift is considerably higher than for a monoplane wing. The neighboring lifting planes of the grid fin induce a more favorable alignment of the flow. This delays the separation to higher angles of attack and causes a smooth separation at supercritical angles. The presence of orthogonal planes avoids the crossflows and gives a good basis to apply the linear theory. Each plane of a grid fin corresponds to a high-aspect-ratio wing. Another simplification of the theoretical model is the independence of the load capacity of a lattice wing (for given plane spacing and wing sizes) on the internal arrangement of the grid (framework or honeycomb). This hypothesis is valid for all wings with a large number of cells ($n > 10$). Therefore, each cell of the wing is considered to be a square box shaped wing, and its internal flow has an aerodynamic behavior that is completely independent. The main geometrical parameters of the lattice wing are the height h, the span b, the plane thickness c, and the distances between the neighboring vertical and horizontal surfaces t_y and t_z. Usually, the distances between the surfaces in a lattice wing are chosen in such a way that $t_z = t_y = t_{yz}$. These grid fin qualities simplify the calculation of the induced aerodynamic forces for the different flow regimes. A sufficiently exact prediction of the performance of these wings, at any angle of attack and yaw, is performed through a simplified formulation of the flow around the lattice wing at different speed ranges. The limits of these speed ranges can be clearly defined by characteristic flow phenomena and determined as functions of the geometrical parameters. The different speed ranges, separated by two critical Mach numbers, M_{cr1} and M_{cr2}, are the subsonic ($M \leq M_{cr1}$), transonic ($M_{cr1} \leq M \leq M_{cr2}$), and supersonic regimes (when $M \geq M_{cr2}$). The supersonic regime itself is split in two by a third critical Mach number M_{cr3}. Above this last critical Mach number, the shock and expansion waves inside the grid fin do not impact on the neighboring planes. The aerodynamic forces induced by lattice wings are calculated for each regime using flow conditions and geometrical parameters.

At subsonic speeds, the calculation model is based on the lifting line scheme. The lift of the lattice wing is computed in two steps. First, each individual plane of the grid fin is supposed to be under the same conditions as those of the corresponding polyplanes with infinite span at the same effective angle of attack. Given the lattice wing dimensions, the aerodynamic coefficients are determined using semiempirical correlations. Then, the axial component induced by the lift has to be estimated. The lift of the grid is approximated as equal to the lift of the corresponding polyplane of infinite span.

The angle of attack of the corresponding polyplane of infinite span is determined by taking into account the average downwash angle from the free vortices of the grid. Afterward, the induced drag of the wing, as well as the friction drag, are calculated. An additional semiempirical correction of the aerodynamic coefficients is determined by considering the real lattice wing dimensions.

For example, the axial coefficient of a lattice wing in a subsonic flow without flow separation is the sum of the axial friction c_{x_f} and lift c_{x_i},

$$c_x = c_{x_f} + c_{x_i} \tag{1}$$

where the contribution of the friction is calculated from the skin-friction coefficient c_f. As an example, for a honeycomb wing,

$$c_{x_f} = 2c_f\left[1 + \frac{h(b + t_{yz})}{b(h + t_{yz})}\right] \tag{2}$$

where c_f is computed using the usual relations valid for boundary layers. The correlations of Young[26] and Van Driest[27] are used for, respectively, laminar and turbulent flows. This modeling is valid until the first critical Mach number M_{cr1} is reached in a grid cell.

The model for transonic flows is applied when the sonic speed is reached in the narrowest cross section of the wing. This corresponds to the critical Mach number M_{cr1}. A restructuration of the flowfield takes place inside the grid fin at this regime, characterized by the formation of strong shock waves and local supersonic zones. This involves an increase of the axial force of the wing through an additional wave drag c_{x_w}, which comes additionally to the known parts of Eq. (1),

$$c_x = c_{x_f} + c_{x_i} + c_{x_w} \tag{3}$$

The axial wave drag of the lattice wing c_{x_w} can be split in two components, one from inside the flow and the other from outside. Both parts are calculated with different simplified theoretical models adapted using empirical equations.

The following physical model is applied for the calculation of the lift coefficient. The analogy between the flow inside the grid cells and the one-dimensional channel flow is used. It is well known that after the achievement of the sound speed in the throat of a convergent–divergent channel, the conditions also remain critical at higher subsonic speeds. As a consequence, the incoming flow upstream of the channel intake is isentropically braked by the upstream influence until the critical Mach number M_{cr1} is reached. This involves the reduction of the mass flux through the channel throat. These conditions can be calculated, and the effect on the lift coefficient determined by comparison with the reference value at M_{cr1} using the relationship of the dynamic pressures at the channel entrance and in the undisturbed incoming flow. Finally, it is demonstrated that the variation of the normal force with the Mach number of the main flow ($M_{\text{cr1}} \leq M \leq 1$) or the subsonic flow behind the head wave ($1 \leq M \leq M_{\text{cr2}}$) is proportional to the variation of the dynamic pressure. The total drag of the wing is increased additionally by the wave drag, which can be calculated using an empirical correlation depending on the wing geometry.

With the achievement of the supersonic regime in the incoming flow at $M \leq M_{\text{cr1}}$, a normal head shock wave moves upstream of the wing. There is no change in the flow inside the grid cells because the flow behind this head wave is subsonic. The wing drag changes because the strong shock wave leads additionally to total pressure losses.

The supersonic regime begins when the second critical Mach number M_{cr2} is reached. At this regime, the head shock wave becomes attached to the leading edges of the planes. The definition of M_{cr2} used in this work corresponds to a higher Mach number, at which the flow becomes supersonic in the complete flowfield between the neighboring planes. In the region where $M > M_{\text{cr2}}$, the flow between two planes of the lattice wing at moderate incidence angles can be calculated with analytic equations. Given the emerging interactions of expansion fans or shock waves in different combinations together or with solid walls, the pressure distributions on the wing surface and the induced forces (without friction drag) can be determined. As a result of the mutual interaction between the planes, the lift coefficient of the lattice wing in this region is reduced, comparing to the typical value for isolated planes. The axial force coefficient can be calculated as

$$c_x = c_{x_f} + c_{x_p} \tag{4}$$

where c_{x_p} is provided by the integration of the surface pressure. The friction component c_{x_f} is calculated as it is at smaller Mach numbers. For a honeycomb wing, Eq. (2) can be used.

At higher Mach numbers, another critical Mach number is reached, M_{cr3}. Above this Mach number, the shock waves and the expansion waves do not impact on the neighboring planes. The surface pressure distribution on each wall is independent and corresponds to the one of an isolated plane. Therefore, the previous physical model remains valid and is applied for the calculation of the force coefficients. The semiempirical module has been validated with experimental data for different grid fin designs.[16,18] It is valid from Mach 0.3 to 6 and until a 90-deg angle of attack.

Integration of the Actuator Disk

The actuator disk just described has been integrated in the unstructured solver TAU, and the module based on the semiempirical theory for grid fins has been coupled with the code.

Each lattice wing of the missile in Fig. 1 is replaced by a set of boundary conditions. The actuator disk has exactly the same size and shape as the external frame of the grid fin. Because it was not possible to use a mesh interface with the unstructured solver and, therefore, a two-dimensional actuator disk, the grid fin thickness has been retained. On the sides of the grid fin, supersonic outflow conditions are applied. Previous simulations for an isolated grid fin have shown that, for subsonic flows, an inviscid wall is valid, but this boundary condition produces a shock in transonic and supersonic flows. The presence of this shock induces additional drag and lift that have no reason to exist because the total contribution of the grid fin (including the external frame), in term of forces, is already taken into account by the actuator disk. This is the reason why a supersonic outflow condition is applied. The use of this boundary condition on the side of the grid fin has been already applied and validated for an isolated grid fin and a wide range of Mach numbers and angles of attack.[22] Only the grid fin arm (Fig. 2) is neglected for the computations.

The actuator disk consists of two surfaces with a priori two different meshes. To apply the actuator disk boundary conditions, each point of a boundary uses the values of the flow variables on the other boundary. As a consequence, for each computational point of an actuator disk side, a mirror point has been created on the other side. At the mirror point, the values of the necessary variables are interpolated from the neighboring points. On the upstream and downstream surfaces, the relevant actuator disk boundary conditions are applied. This is done for each point of the surfaces.

Downstream of the grid fin, the flow has been modified. By the use of the semiempirical module, based on lattice wing theory, the local aerodynamic forces induced by the grid fin are calculated as functions of the local flow conditions (Mach number, angles of attack, and yaw) and grid fin geometrical characteristics (height, chord, span, spacing, and plane thickness). This is done for each point of the actuator disk downstream surface. In this way, all of the local flow perturbations are accounted for. This is particularly efficient when taking into account the local effects due to the interactions between the fins and the body.

The final code has been already applied on an isolated grid fin.[22] This has demonstrated the capability of the tool to reproduce, for this geometry, the trends of the force coefficient evolution for a wide range of Mach numbers (from Mach 0.8 to 4) and angles of attack (from 0 to 20 deg). Here, the tool is applied to the simulation around a complete missile to determine the influence of the grid fins on the vehicle overall performances.

Application to Missile

Computational Conditions

The missile with grid fins computed here has already been experimentally investigated at DLR Cologne.[18] The geometry is

Table 1 Mach and Reynolds numbers, angles of attack, and boundary-layer modeling of different computed cases for complete vehicle and body alone

Case	Mach number	Reynolds number	Angle of attack	Approach
1	1.8	1.8×10^6	0	Laminar
2	1.8	1.8×10^6	0	Wilcox[a]
3	2	1.9×10^6	0	Wilcox
4	3	2.5×10^6	0	Wilcox
5	4	3.3×10^6	0	Laminar
6	4	3.3×10^6	0	Wilcox
7	4	3.3×10^6	0	Spalart–Allmaras[b]
8	4	3.3×10^6	5	Wilcox
9	4	3.3×10^6	10	Wilcox
10	4	3.3×10^6	20	Wilcox

[a]Turbulence model Wilcox is two-equation k–ω model.
[b]Turbulence model Spalart–Allmaras's one-equation model.

represented in Figs. 1 and 2. The same grid fin, taken isolated, had been previously retained to validate the numerical tool.[22] In the wind-tunnel tests, the model is maintained by a support that is not taken into account for the computations. Note that this support is fixed on the missile base but does not fit the base exactly. The length of the missile is 480 mm, and its diameter 52 mm. The missile has a sharp nose, and the length of the cylindrical afterbody is 350 mm. The lattice wings are located 30 mm from the base and are maintained close to the body by four arms that are neglected in the numerical simulations. Because of the symmetry of the configuration, only one-half of the missile has been computed. To assess the influence of the lattice wings on the numerical results, a body alone has been also computed. This body corresponds to the vehicle just described without grid fins.

The geometries described have been computed at Mach numbers 1.8, 2, 3, and 4. The different cases with the corresponding Mach and Reynolds numbers and angles of attack are shown in Table 1. Computations have been performed for laminar and turbulent flows. For the turbulence modeling, two models have been tested, the Spalart–Allmaras one-equation model and the two-equation k–ω model of Wilcox. Because the objective of this work is to develop a tool devoted to the design of high-supersonic (or low-hypersonic) vehicles with grid fins, the computations with angle of attack have been performed at Mach 4. Three cases at 5-, 10-, and 20-deg angles of attack have been computed to check the reliability of the tool in the presence of angle of attack. Case 6 of Table 1 has been computed for the current configuration, but also for the same missile with different grid fins, to evaluate the code capabilities to be used as design tool for a vehicle with grid fins.

The boundary conditions applied to the computational domain are as follows: The walls are isothermal, the plane $y = 0$ is the symmetry plane, and the other boundaries are the far field. For the complete vehicle, at the lattice wing locations, the actuator disk conditions are applied.

Meshes

The meshes used to simulate the missile and the body alone have been generated with the CENTAUR[28] grid generator. For both configurations (Figs. 6 and 7), the computational domains extend over a little more than one-half of the vehicle length in the transverse direction and one-third of the vehicle length downstream of the base.

For each configuration, a first grid has been created, then adapted, adding new cells using the adaptation module of TAU[21] and a gradient-based approach. This process has been carried out until the achievement of grid convergence. The procedure of adaptation can be described as follows. With a first grid, a first computation is performed, then the mesh is adapted at the shock until a constant value of the force coefficients is reached. In the second step, the mesh is converged for the complete vehicle. The last step is the optimization of the mesh in the boundary layer; this is achieved with a y^+ value lower than 1. During the mesh adaptation process, at each adaptation loop, 10% more points were added. For the body,

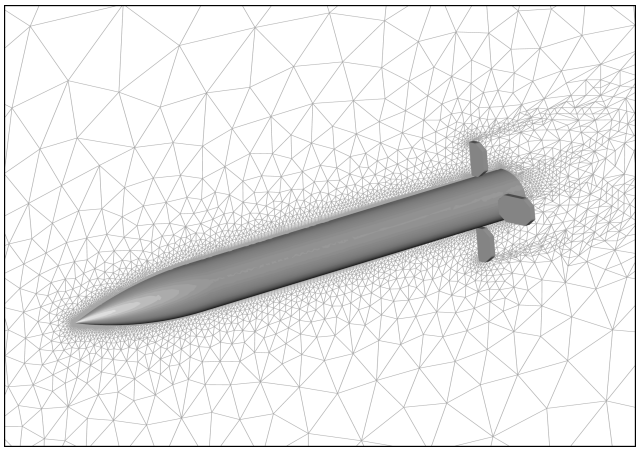

Fig. 6 Symmetry plane of hybrid mesh used to compute complete vehicle.

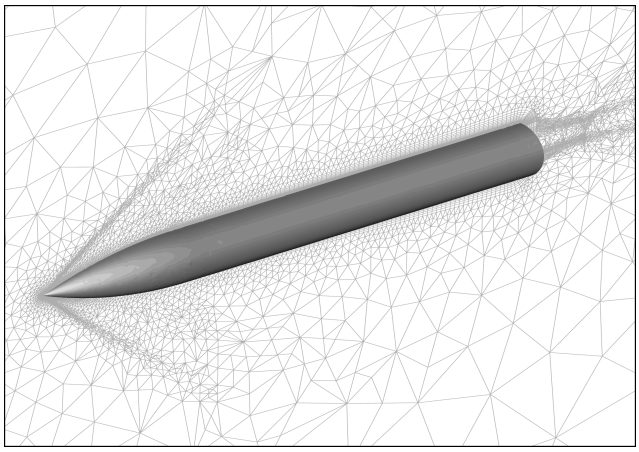

Fig. 7 Symmetry plane of hybrid mesh used to compute body alone.

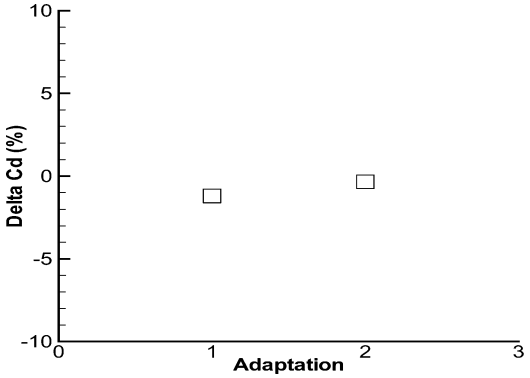

Fig. 8 Evolution of drag of complete missile, in percent, during mesh adaptation process for laminar flow at Mach 4.

a quite coarse mesh was initially used, and around 12 adaptations were necessary to reach the grid independence of the results. For the complete vehicle, the initial mesh was much finer, and from two to four adaptations were sufficient.

The results obtained for the successive adaptations of the mesh of the complete vehicle for a laminar flow at Mach 4 are shown in Fig. 8. In Fig. 8, the drag variation in percent is plotted. To adapt the mesh, only two adaptations were necessary, for a total increase of 20% of the points. At the second adaptation, the drag was approximately the same as the first one, with a variation lower than 0.5%. Therefore, the mesh was considered to be converged for this case. The final meshes obtained at Mach 4 and laminar conditions, for the body alone and the complete vehicle, are shown in Figs. 6 and 7. To

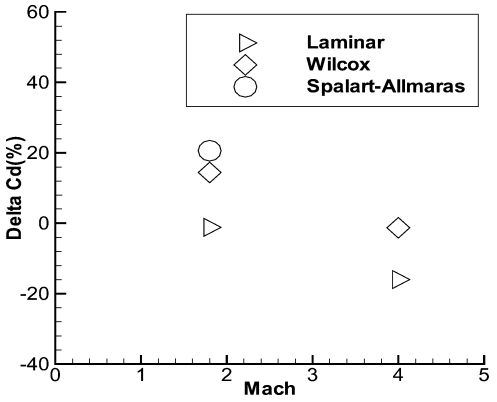

Fig. 9 Differences in percent between experimental and numerical values of drag for body alone at Mach 1.8 and 4.

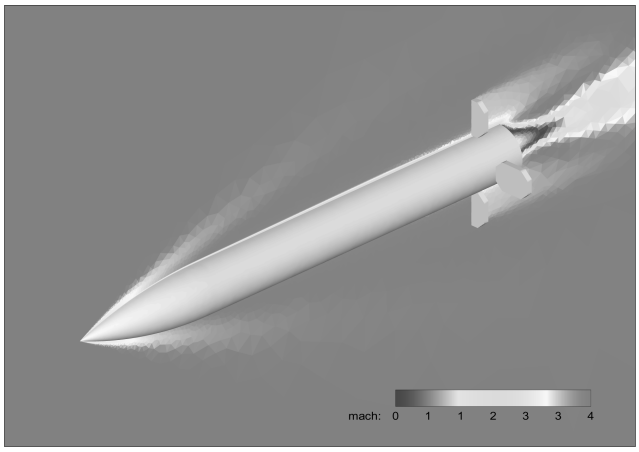

Fig. 10 Mach number distribution around complete missile at Mach 4 without angle of attack and with k–ω Wilcox turbulence model.

save some effort, these meshes have been used as starting meshes for the other computations in Table 1; then, of course, the same process of mesh adaptation has been carried out. The final mesh for the complete vehicle, shown in Fig. 6, is approximately 400,000 tetrahedra and 560,000 prisms. For the body alone, the mesh (Fig. 7) is around 440,000 tetrahedra and 490,000 prisms. This demonstrates that, when the actuator disk concept is used, the size of the mesh required for the complete vehicle is almost the same as that for a body alone. When the complete vehicle is computed without the actuator disk approach, the mesh is at least five times larger than for a body alone.

Vehicle Without Angle of Attack

Cases 1–7 of Table 1 correspond to the computations of the vehicle and the body alone at zero angle of attack. Because the multigrid technique is available with TAU,[21] two grid levels have been used for the computations. The computations have been started using the coarse grid and finished with the fine grid to save some computational effort. The Courant–Friedrichs–Lewy numbers used for the simulations varied from 2 for a laminar flow without angle of attack to 0.5 for the turbulent predictions at a 20-deg angle of attack. With dependence on the computed case, between 15,000 and 30,000 iterations were required to achieve the result convergence using the AUSM-DV numerical scheme integrated in TAU.[21]

First, the influence of the turbulence modeling was checked for a body alone. In Fig. 9, the differences in percent between the numerical results and the experimental data[18] obtained for the drag of the complete body, including the base C_d, are shown. The simulations show a very good agreement between the laminar prediction and the experimental data at Mach 1.8. The drag is overestimated by both turbulent calculations. The Wilcox k–ω model provides a value of the drag of 14% from the experimental value. This is not the case of the calculation with the model of Spalart–Allmaras where the difference with the experiments is around 20%. For this reason, this model has not been used in the other computations. At Mach 4, the experimental data are underestimated by the laminar prediction, whereas the k–ω model provides good agreement. The experimental data[18] have been obtained for flows that become turbulent at the shoulder of the missile. Moreover, this study is dedicated to high-supersonic flows. Therefore, the approach with the k–ω Wilcox model has been selected for all of the computations of both body alone and complete missile. The discrepancies observed between the experiments and the numerical simulations are small (an order of 10%) and may originate from two sources. First, the turbulent boundary layer might not be fully developed on the body. Second, the wind-tunnel model support is not taken into account. However, this support is only fixed on a portion of the base, and its contribution to the drag should be small.

The complete missile has been computed at Mach 1.8, 2, 3, and 4 with the k–ω Wilcox model. The Mach number distribution around the vehicle at Mach 4 is shown in Fig. 10. To cancel the influence of the wind-tunnel model support, instead of comparing the experimental and the numerical values of the drag for the complete vehicle, the comparisons are based on the differences between the drags of the complete vehicle and the body alone obtained experimentally and numerically, which are shown in Fig. 3. The results obtained in the past[19] are also reported in Fig. 3. The improvement of the numerical results when using the semiempirical module instead of an experimental database is obvious. Before, when the actuator disk technique was used, it was possible to recover more than 75% of the differences between the drag of the missile and the body alone. Now, the predictions are much better. For all cases the simulations recover more than 90% of the grid fin effects. This demonstrates that the semiempirical module is more capable of taking into account local flow deviations in terms of velocity and angles induced by the presence of the body and by the interactions between the grid fins and the body. However, even with the semiempirical module, the technique does not recover 100% of the differences. In this study, there is another source of discrepancy. The semiempirical theory for lattice wings, used here, is adapted to fins with uniform cells. Because some cells of the current grid fin differ in shape (Fig. 2), its drag is underestimated. This was also the case for the same isolated lattice wing in a previous work.[22] The grid cells close to the base are smaller than the others; this involves more honeycomb elements than in a uniform grid. Because the semiempirical theory is adapted to grid fins with uniform cells, the calculations of the grid fin coefficient is performed with a model valid for a grid with fewer honeycomb elements. As a consequence, the drag of the lattice wing of Fig. 2 is underestimated. This explains why the code is not able to recover completely the lattice wing effects.

Design Capabilities

To assess the capabilities of the code for design analysis, the complete missile has been computed with different grid fins. The vehicle is still equipped with honeycomb grid fins as in Fig. 1, but the new fins have thinner inner and outer frame thicknesses. The configuration has been computed for case 6 of Table 1. The differences between the drag of the complete missile and the body alone are shown in Fig. 11. The results show that using another geometry (thin grid fins) for the lattice wings, the additional drag of the complete vehicle due to the lattice wings can be considerably tailored, here, by a factor of three. The convergence of the numerical results is obtained after some hundreds of iterations and without additional mesh generation effort. This demonstrates the usefulness of the tool for system analysis during the design loops of vehicles equipped with such devices.

Furthermore, from a design point of view, an important capability of the tool is to predict the same trends as observed in the experiments. Figure 3 shows that the numerical results predict, as in the experiments, a drag reduction by almost a factor two when the Mach number increases from 1.8 to 4. This demonstrates the validity of

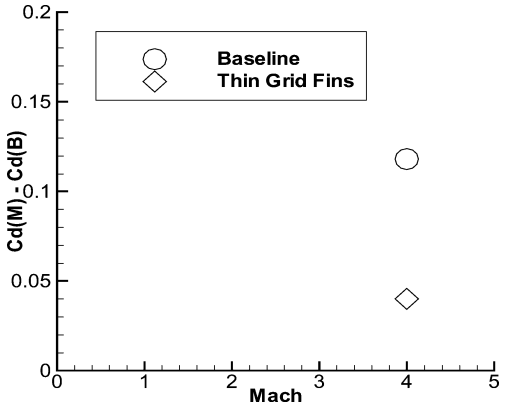

Fig. 11 Differences between drags of complete missile and body for current lattice wings and for thinner grid fins at Mach 4.

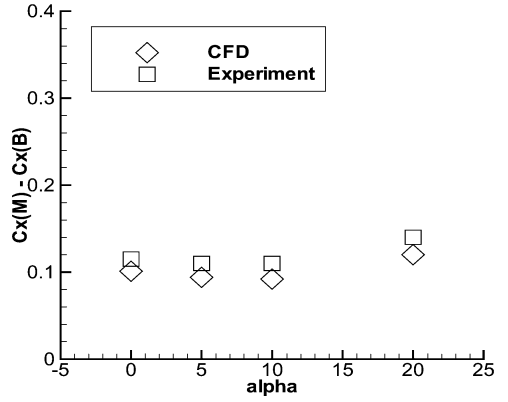

Fig. 12 Differences between axial force coefficients of complete missile and of body alone as functions of angle of attack.

the actuator disk to predict the force changes on a vehicle with grid fins for different Mach numbers and without angle of attack.

Presence of Angle of Attack

To assess the validity of the method in the presence of angle of attack, several computations have been performed for 5-, 10-, and 20-deg angles of attack. These calculations are reported in Table 1 as cases 8 to 10. Because the objective is to develop a numerical tool for high-supersonic Mach numbers, the computations with angle of attack have been performed at Mach 4 and not at Mach 1.8, as was done previously.[20] Both complete vehicle and body alone have been computed. The predictions for the body alone are used as a reference for estimating the capabilities of the actuator disk. In a previous contribution,[24] the predictions of the axial and normal forces for both body alone and complete missile were found to be in good agreement with the experimental data for all angles of attack. Here, the focus is on the actuator disk capabilities to recover the differences in aerodynamic coefficients between the complete missile and the body alone. For this purpose, the differences between the values predicted for the complete missile and for the body alone in the simulations and in the experiments are shown in Fig. 12 for the axial force, Fig. 13 for the normal force, and Fig. 14 for the pitching moment. The pitching moment has been calculated taking the neutral point of the missile as reference point. Figure 12 shows good agreement at all angles of attack between the evolution of the axial force found experimentally and numerically. More than 90% of the differences between the axial forces of the missile and the body alone are recovered. The experimental difference is generally slightly underestimated. As for the results without angle of attack (Fig. 3), this is because the lattice wing used here differs in shape from the one modeled using the semiempirical theory.

In Fig. 13, the same comparison for the normal force displays good agreement except for a discrepancy at a 5-deg angle of attack. However, the actuator disk is able to reproduce fairly well the evolution of the forces with the angle of attack. This demonstrates the efficiency of the numerical tool in recovering the forces for the complete vehicle in the presence of angle of attack. The results for the pitching moment are shown in Fig. 14. The results are good, with some small discrepancies at 5 and 10 deg between the differences found experimentally and numerically. Similar to the force coefficients, the tool is able to predict correctly the trend evolution of this quantity.

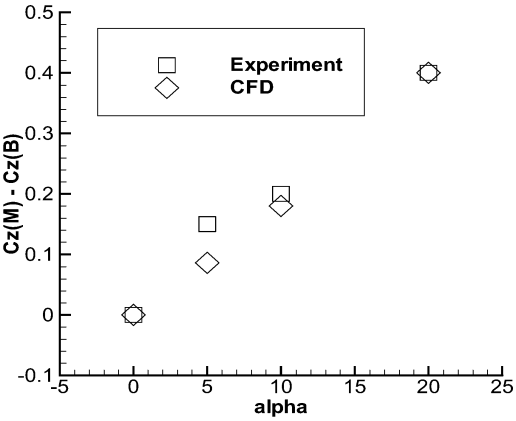

Fig. 13 Differences between normal force coefficients of complete missile and of body alone as functions of angle of attack.

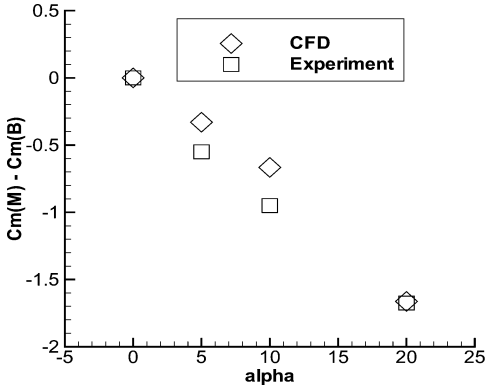

Fig. 14 Differences between pitching moment coefficients of complete missile and of body alone as functions of angle of attack; pitching moment has been calculated taking neutral point (zero angle of attack center of pressure) of missile as reference point.

Conclusions

The objective of this work was to develop a tool for the design of high-supersonic missiles with lattice wings. To this end, an actuator disk for lattice wings already tested with a structured code has been integrated in the unstructured code TAU. Instead of being coupled to an experimental database, the code has been coupled with a numerical module based on the semiempirical theory for lattice wings, providing the force coefficients as a function of flow conditions and grid fin geometry. The complete tool has been applied to a missile with lattice wings. Several computations have been performed for a wide range of Mach numbers and angles of attack. In parallel, a body alone has been computed to be used as reference case for the complete vehicle.

The numerical results demonstrate the validity of the actuator disk approach for the design and the analysis of supersonic vehicles equipped with grid fins. The predictions obtained with the actuator disk coupled with the semiempirical module and those computed previously with an experimental database have been compared. The comparisons for the prediction of the drag coefficient have demonstrated the improvements obtained when using the semiempirical module. These improvements are due to the more extended range

of validity of the semiempirical module, in terms of Mach number, angle of attack, and yaw angle. When the semiempirical module is used, the local flow conditions are taken into consideration better by the numerical tool. This is particularly important to account for the body/grid fin interaction effects. The changes in force and moment coefficients experienced by the missile, due to the presence of the grid fins, are qualitatively and quantitatively very well reproduced compared to the experimental data.

The required computer time for a complete configuration on a workstation is less than 20% more than the time required for a body alone. The extra time corresponds to the additional mesh involved by the presence of the lattice wings and by the actuator disk. Note that a simulation of such a configuration without an actuator disk would require computational effort between four and six times greater than for a body alone. Another advantage of the actuator disk technique is that as long as the grid fin configuration (number of wings, size, and position) remains constant, no additional time for the grid generation is necessary to test different lattice wing geometries. Moreover, the new flow solutions are obtained with little additional computational effort. Compared to a complete simulation without an actuator disk, this means an additional time savings on the order of weeks to analyze the impact of lattice wing geometry on missile performance.

Acknowledgments

The present work was performed in the framework of the DLR Hochagile Flugkörper project. The financial support of the German Ministry of Defence and the project monitoring by H. Ciezki are gratefully acknowledged. This study was partially presented at the International Symposium on Integrating Computational Fluid Dynamics and Experiments in Aerodynamics held in Glasgow on 8 and 9 September 2003. The authors wish to thank the Associate Editor, P. Weinacht, for his advice and suggestions during the review process.

References

[1]Khalid, M., Sun, Y., and Xu, H., "Computation of Flows past Grid Fin Missiles," *RTO MP 5, Proceedings of RTO AVT Symposium on Missile Aerodynamics*, Sorrento, Italy, 1998, pp. 12.1–12.11.

[2]Kretzschmar, R. W., and Burkhalter, J. E., "Aerodynamic Prediction Methodology for Grid Fins," *RTO MP 5, Proceedings of RTO AVT Symposium on Missile Aerodynamics*, Sorrento, Italy, 1998, pp. 11.1–11.11.

[3]Simpson, G. M., and Sadler, A. J., "Aerodynamic Prediction Methodology for Grid Fins," *RTO MP 5, Proceedings of RTO AVT Symposium on Missile Aerodynamics*, Sorrento, Italy, 1998, pp. 9.1–9.11.

[4]Washington, W. D., and Miller, M. S., "Experimental Investigations of Grid Fin Aerodynamics: A Synopsis of Nine Wind Tunnel and Three Flight Tests," *RTO MP 5, Proceedings of RTO AVT Symposium on Missile Aerodynamics*, Sorrento, Italy, 1998, pp. 10.1–10.13.

[5]Brooks, R. A., and Burkhalter, J. E., "Experimental and Analytical Analysis of Grid Fin Configurations," *Journal of Aircraft*, Vol. 26, No. 9, 1989, pp. 885–887.

[6]Burkhalter, J. E., Hartfield, R. J., and Leleux, T. M., "Nonlinear Aerodynamic Analysis of Grid Fin Configurations," *Journal of Aircraft*, Vol. 32, No. 3, 1995, pp. 547–554.

[7]Washington, W. D., Booth, P. F., and Miller, M. S., "Curvature and Leading Edge Sweep Back Effects on Grid Fin Aerodynamic Characteristics," AIAA Paper 93-3480, Aug. 1993.

[8]Belotserkovsky, S. M., Odnovol, L. A., Safin, Yu. Z., Tylenev, A. I., Prolov, V. P., and Shitov, V. A., *Reshetchatye krylia*, Maschinostroenie, Moscow, 1985.

[9]Burkhalter, J. E., and Frank, H. M., "Grid Fin Aerodynamics for Missile Applications in Subsonic Flow," *Journal of Spacecraft and Rockets*, Vol. 33, No. 1, 1996, pp. 38–44.

[10]DeSpirito, J., Edge, H. L., Weinacht, P., Sahu, J., and Dinavahi, P. G., "Computational Fluid Dynamics Analysis of a Missile with Grid Fins," *Journal of Spacecraft and Rockets*, Vol. 38, No. 5, 2001, pp. 711–718.

[11]Lin, H., Huang, J.-C., and Chieng, C.-C., "Navier–Stokes Computations for Body/Cruciform Gridfin Configuration," AIAA Paper 2002-2722, June 2002.

[12]Sun, Y., and Khalid, M., "A CFD Investigation of Grid Fin Missiles," AIAA Paper 98-3571, July 1998.

[13]Fournier, E. Y., "Wind Tunnel Investigation of Grid Fin and Conventional Planar Control Surfaces," AIAA Paper 2001-0256, Jan. 2001.

[14]Lesage, F., "Numerical Investigation of the Supersonic Flow Inside a Cell," *Proceedings of the 17th International Symposium on Ballistics, BALLISTICS'98*, Vol. 1, Midrand, South Africa, 1998, pp. 209–216.

[15]Washington, W. D., and Miller, M. S., "An Experimental Investigation of Grid Fin Drag Reduction Techniques," AIAA Paper 93-0035, Jan. 1993.

[16]Esch, H., "Kraftmessungen an Gitterleitwerken im Überschall," DLR Internal Bericht, IB 39113-99C11, Cologne, Germany, 1999.

[17]Böhm, G., "Aerodynamische Grundlagen und Eigenschaften von Gitterflügeln zur Steuerung von Lenkflugkörper," IABG Bericht, B-WT 4719/02, Ottobrunn, Germany, 1994.

[18]Esch, H., "Aerodynamisches Beiwerte der Längsbewegung eines Flugkörpers mit Gitterleitwerk im Überschall," DLR Internal Bericht, IB 39113-2000C34, Cologne, Germany, 2000.

[19]Reynier, Ph., Reisch, U., Longo, J., and Radespiel, R., "Numerical Study of Hypersonic Missiles with Lattice Wings Using an Actuator Disc," AIAA Paper 2002-2719, June 2002.

[20]Reynier, Ph., Reisch, U., Longo, J.-M., and Radespiel, R., "Flow Predictions Around a Missile with Lattice Wings Using the Actuator Disc Concept," *Aerospace Science and Technology*, Vol. 8, No. 5, 2004, pp. 377–388.

[21]Gerhold, T., Friedrich, O., Evans, J., and Galle, M., "Calculation of Complex Three Dimensional Configurations Employing the DLR TAU Code," AIAA Paper 97-0167, Jan. 1997.

[22]Reynier, Ph., and Schülein, E., "Incorporation of an Actuator Disc for Lattice Wings in an Unstructured Navier–Stokes Solver," *Notes on Numerical Fluid Mechanics and Multidisciplinary Design: New Results in Numerical and Experimental Fluid Mechanics IV*, edited by C. Breitsamber, B. Laschka, H.-J. Heinemann, and R. Hilbig, Springer-Verlag, 2004, pp. 132–139.

[23]Horlock, J. H., *Actuator Disk Theory*, McGraw–Hill, New York, 1978.

[24]Reynier, Ph., Schülein, E., and Longo, J., "Simulation of Missiles with Grid Fins Using an Unstructured Navier–Stokes Solver Coupled to a Semi-Empirical Actuator Disc," *Proceedings of Conference on Integrating CFD and Experiments*, Glasgow, Scotland, U.K., 2003.

[25]Schülein, E., "Expertensystem zur Auslegung und Optimierung isolierter Gitterflügeln," DLR Internal Bericht, Göttingen, Germany, 2003.

[26]Young, A. D., "High Speed Flow," *Modern Developments in Fluid Mechanics*, edited by L. Howard, Vol. 1, Clarendon, Oxford, 1953, pp. 375–475.

[27]Van Driest, E. R., "On Turbulent Flow near a Wall," *Journal of Aeronautical Sciences*, Vol. 23, No. 11, pp. 1007–1011, 1036, 1956.

[28]"Online Users Manual," Centaur Soft, 1997–2005, URL: http:/www.centaursoft.com/support/manual/.

P. Weinacht
Associate Editor